RSC Advances

PAPER

View Article Online
View Journal | View Issue

Cite this: *RSC Adv.*, 2025, **15**, 18237

Antibacterial and electrical performance of triboelectric nanogenerators based on polyhexamethylene guanidine hydrochloride in high humidity environments

Doan T. Tung, [a] Hoang T. Dung, [ab] Le T. T. Tam, [ab] Bui V. Cuong,[a] Ha M. Dung,[c] Duong V. Dat,[c] Ngo T. Dung, [a] Nguyen T. Dung,[a] Phan N. Minh*[b] and Le T. Lu *[ab]

A humidity-resistant, antibacterial triboelectric nanogenerator (TENG) was developed using polyhexamethylene guanidine hydrochloride (PHMG) as the primary functional material. To enhance performance stability, PHMG was integrated with natural chitosan (CS) to create a positively charged triboelectric electrode. When combined with a negatively charged fluorinated ethylene propylene (FEP) membrane, the TENG demonstrated outstanding electrical output, achieving a maximum peak-to-peak voltage (V_{p-p}) of 1470.6 V and a peak power (P_{peak}) of 12 mW at a 10 MΩ load under 40% relative humidity. Notably, the device maintained stable operation in high-humidity conditions (up to 90% HR), with a sustained V_{p-p} of 862.7 V and a P_{peak} of 6.5 mW. In addition to its energy-harvesting capability, the TENG exhibited strong antibacterial activity as it effectively eliminated *E. coli* (at a concentration of 1.7×10^4) and *S. aureus* (at a concentration of 1.6×10^4) bacteria within just 60 seconds at 90% relative humidity. This combination of reliable triboelectric generation in humid environments and rapid antibacterial activity indicates the potential of this TENG for self-powered applications in wearable electronics and hygienic surfaces, including smart face masks and antibacterial shoe insoles.

Received 19th April 2025
Accepted 25th May 2025

DOI: 10.1039/d5ra02735g

rsc.li/rsc-advances

Introduction

Triboelectric nanogenerators have attracted increasing attention as self-powered platforms for antibacterial applications, due to their ability to convert mechanical energy into electrical energy without relying on external power sources.[1,2] This feature enhances the energy efficiency of the system, while also offers several advantages, including cost-effective design, high versatility, and mechanical durability under repeated operational conditions.[3–8] In addition, their lightweight and flexible nature allows for facile integration with the human body, rendering them highly suitable for wearable and biomedical applications.[9–11] Nevertheless, several challenges remain in the practical application of TENGs for antibacterial purposes. In particular, the high-humidity conditions often encountered in real-world scenarios can reduce device performance. This issue is especially critical in healthcare-related applications, such as face masks and medical devices, where both energy generation and antibacterial efficacy are essential.[12,13] Therefore, the development of TENGs with enhanced and stable antibacterial functionality is of considerable interest for expanding their applicability in biomedical and clinical settings.

To address the growing demand for antibacterial performance, numerous studies have explored the integration of functional nanomaterials into TENGs. These materials include inorganic nanoparticles (*e.g.*, Ag, TiO_2, ZnO, Te)[13–19] and organic antibacterial agents (*e.g.*, cationic polymers).[20–24] For example, Lin *et al.* developed a TENG using tellurium nanowire (Te NW) coated on carbon fiber, followed by a thin gold layer to enhance electrical conductivity. The resulting system employed a dual antibacterial mechanism involved electroporation (electrical pulse-induced membrane disruption) and controlled hydrogen peroxide (H_2O_2) production, which effectively eliminated bacterial during TENG operation. Notably, this design achieved bactericidal efficiencies of 87% against *S. aureus* and 96% against *E. coli* at a frequency of 4 Hz after 60 minutes of operation.[13,19]

In another study emphasising environmental sustainability, Long Gu's research group reported the fabrication of a high-performance TENG using recycled PET combined with antibacterial polymer PHMG. The PET-PHMG nanofiber membrane, fabricated through electrospinning, served as the positive triboelectric layer, while a polyvinylidene fluoride (PVDF) membrane was employed as the negative counterpart.

[a]*Institute of Materials Science, Vietnam Academy of Science and Technology, 18 Hoang Quoc Viet, Hanoi, Vietnam. E-mail: pnminh@vast.vn; lult@ims.vast.ac.vn*

[b]*Graduate University of Science and Technology, Vietnam Academy of Science and Technology, 18 Hoang Quoc Viet, Hanoi, Vietnam*

[c]*VNU University of Engineering and Technology, VietNam National University, 144 Xuan Thuy Road, Cau Giay, Ha Noi, Vietnam*

The device achieved a peak output voltage of 120.2 V, current of 2.9 μA, and charge density of 22.1 nC cm^{-2}, among the highest values reported for TENGs derived from waste materials.[22] Moreover, the device exhibited stable operation over 2500 test cycles and demonstrated effective antibacterial activity against *S. aureus* and *E. coli*.

Cationic polymers combined with polysaccharides have attracted increasing interest due to their intrinsic antibacterial properties, environmental friendliness, and high biocompatibility.[25–27] Among these, the combination of chitosan and PHMG has been widely employed in the development of antibacterial coatings and membranes.[28,29] In addition to their antimicrobial activity, both chitosan and PHMG exhibited strong positive triboelectric properties.[22,24,30,31] However, reports on the integration of PHMG and chitosan specific for antibacterial TENG remain very limited.

In this study, we report the development of a novel antibacterial TENG capable of maintaining high performance under elevated humidity conditions (up to 90% RH). The device features an innovative design in which the positive electrode membrane is fabricated through integration of naturally-derived chitosan polymer (CS) with PHMG, utilising glutaraldehyde (GA) as a cross-linking agent. This composite material leverages the biocompatibility and environmental sustainability of chitosan, while harnessing the potent antibacterial activity of PHMG. The negative triboelectric electrode is constructed using a FEP membrane, creating an efficient interface for charge separation. This configuration enables dual functionality, providing both robust triboelectric output and enhanced bactericidal performance. The TENG exhibits outstanding electrical characteristics, achieving a peak-to-peak open-circuit voltage, V_{p-p} of 1470.6 V and a maximum power output, P_{peak} of 12 mW under ambient conditions. Notably, the device maintains remarkable operational stability in high-humidity environments, generating a V_{p-p} of 862.7 V and P_{peak} of 6.5 mW at 90% relative humidity, while preserving its antibacterial efficacy.

Experimental

Materials

Guanidine hydrochloride (GHC, CH_5N_3HCl, 99%), hexamethylene diamine (HMDA, $C_6H_{16}N_2$, 99%), glutaraldehyde (GA) solution in water (50% concentration), isopropyl alcohol and acetic acid (99.7%) were purchased from Sigma-Aldrich. Chitosan (CS) with standard molecular weight was obtained from Vietnam Food Joint Stock Company.

Copper adhesive tape, sourced from Korea, had a thickness ranging from 0.05 to 0.06 mm. Commercial transparent fluorinated ethylene propylene (FEP) film, approximately 0.1 mm thick, was obtained from materials commonly used in Anycubic MONO X 3D printers.

Preparing for chitosan–PHMG–GA (CS–PHMG–GA) solution

PHMG was synthesised according to our previous study.[24] GA was then added to the PHMG solution at a concentration of 25% relative to PHMG by weight, and the mixture was stirred at 60 °C for 6 hours. Separately, CS flakes were completely dissolved in 2% (v/v) acetic acid by vigorous stirring at 60 °C until a clear and homogeneous solution was obtained. Degassing was performed to remove any trapped air bubbles.

The CS–PHMG–GA mixture was prepared by combining the PHMG–GA solution with the chitosan solution in various mass ratios of CS : PHMG–GA, specifically 9 : 1, 8 : 2, 7 : 3, 6 : 4, and 5 : 5. These samples were labeled C9P1, C8P2, C7P3, C6P4, and C5P5, respectively. During the preparation, 1 mL of isopropyl alcohol was first mixed with the PHMG–GA solution before being added to the CS solution, and the entire mixture was stirred thoroughly to ensure uniform blending.

Fabrication of TENG electrode and test system

The CS–PHMG–GA-based TENG electrodes were fabricated using the doctor blade technique. The CS–PHMG–GA gel was directly coated onto a 10 × 10 cm^2 copper adhesive tape substrate. The coated electrodes were then dried in an oven at 80 °C overnight to ensure complete solvent evaporation. The TENG device features a simple vertical contact–separation structure composed of two friction electrodes. The positive electrode consists of the dried CS–PHMG–GA membrane on copper tape, while the negative triboelectric electrode is a FEP film also mounted on copper adhesive tape. Both electrodes were assembled on a spring-supported system with a mounting base made from white PVC plastic sheets, as illustrated in Fig. 1.

To investigate the device performance under various environmental conditions, the entire TENG module was enclosed in a sealed polycarbonate (PC) chamber. This setup allowed precise control of relative humidity levels and bacterial exposure conditions for comprehensive performance evaluation.

Characteristics

FTIR spectra were recorded using a Nicolet 6700 FT-IR spectrometer in the wavenumber range of 4000–400 cm^{-1} to identify the functional groups present in the materials. The surface morphology and elemental composition of the TENG electrode were examined using a field emission scanning electron microscope (FE-SEM, HITACHI) equipped with an energy-dispersive X-ray spectroscope (EDX).

The open-circuit voltages (OCV or VOC) and load voltages of the TENG device were characterised using Lecroy Wave Surfer 424 oscilloscope. The load currents were indirectly measured through the voltage divider resistor (shunt resistor) by Instek GDS-806S digital storage oscilloscope.

Regarding antibacterial properties, two bacterial strains, *Escherichia coli* ATCC 25922 (*E. coli*) and *Staphylococcus aureus* ATCC 6538 (*S. aureus*), were cultured on tryptic soy agar (TSA) plates for 32 hours. Bacterial cells were harvested using sterile 0.9% NaCl solution and adjusted to a final concentration of 10^7 CFU mL^{-1}, standardised according to the McFarland method. A 0.2 mL aliquot of each suspension was evenly spread onto the surface of electrode samples (bare Cu and Cu coated with CS–PHMG–GA of 4 × 4 cm) using sterile cotton swabs. The inoculated samples were then air-dried under aseptic conditions in

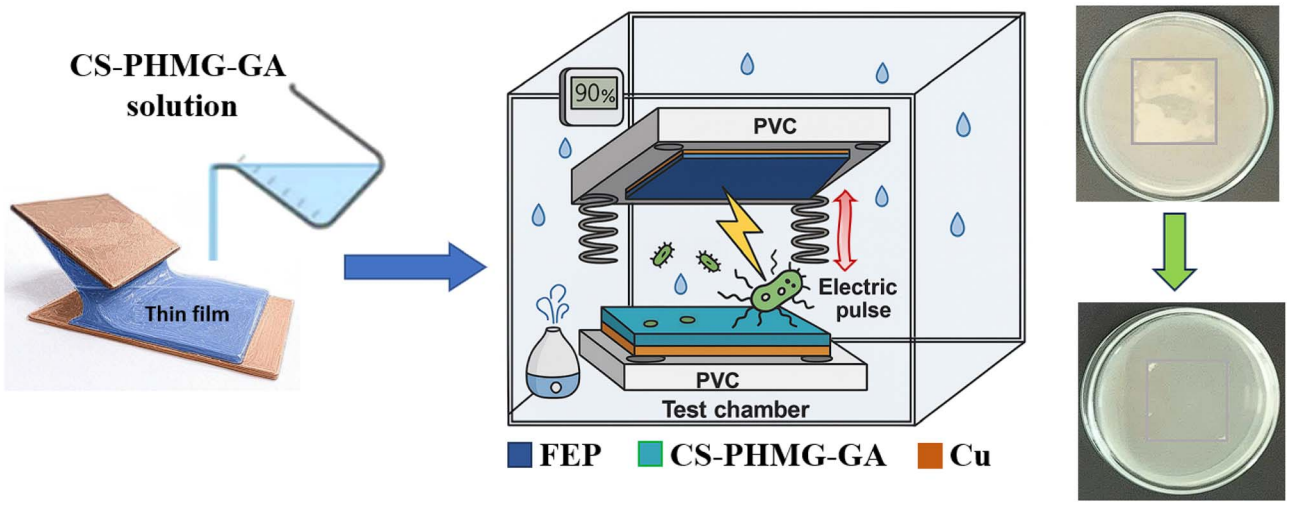

Fig. 1 Schematic illustration of the fabrication process and high bactericidal ability during operation of CS–PHMG–GA based TENG.

a laminar flow cabinet for 60 minutes prior to pulsed electric treatment.

The inoculated electrode samples were employed as the positive electrode in the TENG setup operating in contact–separation mode for various time intervals. Following triboelectric pulse exposure, antibacterial activity was assessed using two methods: (i) quantitative colony-forming unit (CFU mL^{-1}) analysis based on ISO 7218:2024 guidelines, and (ii) the direct agar imprint method (the dried inoculated samples were pressed onto agar plates for 15 min and then removed). All treated and control samples were incubated at 30 °C for 24 hours. Control samples, which were inoculated identically but not subjected to triboelectric pulses, served as negative controls for comparison of bactericidal efficiency.

Results and discussions

Polymer composite material properties

The CS–PHMG–GA membrane demonstrates high optical transparency and strong adhesion to the copper foil substrate, as shown in Fig. 2. The SEM image of the sample reveals a relatively uniform surface morphology, free from large pores or visible defects, indicating successful membrane formation and uniform coating over the copper surface.

EDX analysis confirms the presence of C, O, N, and Cl elements, corresponding to the major components of CS, PHMG, and GA, along with a small amount of copper (Cu) from the substrate was also detected (Fig. 2c and d). The elemental composition was approximately 51.8% C, 22% O, 17% N, 4.9% Cl, and 4.2% Cu. The relatively high nitrogen content is attributed to contributions from both CS and PHMG, which is favorable for enhancing the positive triboelectric performance of the electrode. Moreover, EDX elemental mapping reveals a uniform distribution of C, N, O, and Cl across the membrane surface, indicating homogeneous dispersion of PHMG and GA within the chitosan matrix.

Fig. 3 shows the FTIR spectra of pure CS, PHMG–GA, and CS–PHMG–GA composite membranes prepared at varying mass ratio of CS to PHMG–GA. The spectrum of pure CS exhibited typical features, including a broad absorption band in the region of 3300–3100 cm^{-1} corresponding to the stretching vibrations of –OH and $-NH_2$ groups. A peak at approximately 2900 cm^{-1} is attributed to C–H stretching vibrations. Additional prominent peaks are observed at 1635 cm^{-1} (C=O stretching, amide I), 1539 cm^{-1} ($-NH_2$ bending), and in the region of 1000–1100 cm^{-1}, which corresponds to the saccharide backbone vibrations.

For the PHMG–GA sample, distinctive peaks appear at 1500–1700 cm^{-1}, assignable to the C=N stretching vibration within the guanidine group, and at 2800–2900 cm^{-1}, corresponding to C–H stretching of the methylene units. As the PHMG–GA content increased from a CS : PHMG–GA mass ratio of 9 : 1 to 5 : 5, several notable spectral changes were observed. These include a gradual reduction in the relative intensity of the broad –OH/$-NH_2$ absorption band, and an increase and slight shift in the peak near 1650–1700 cm^{-1}, and a noticeable shift in the region around 1550 cm^{-1}. These spectral modifications indicate molecular interactions between the guanidine moieties of PHMG–GA and the carboxyl or amino groups of chitosan, most likely *via* ionic bonding.

Furthermore, the emergence or enhancement of the band at ~1650 cm^{-1} suggests the formation of imine bonds (C=N), arising from reactions between aldehyde groups of glutaraldehyde (GA) and amine groups in either CS or PHMG. However, due to the overlap of amide I and C=N stretching regions, unambiguous assignment of this peak remains challenging.

Triboelectric properties

Fig. 4a illustrates the variation in V_{OC} output of the TENG device fabricated with different CS : PHMG–GA mass ratios. As the proportion of PHMG–GA increases, the amplitude of V_{OC} oscillation exhibits a progressive enhancement. This trend is

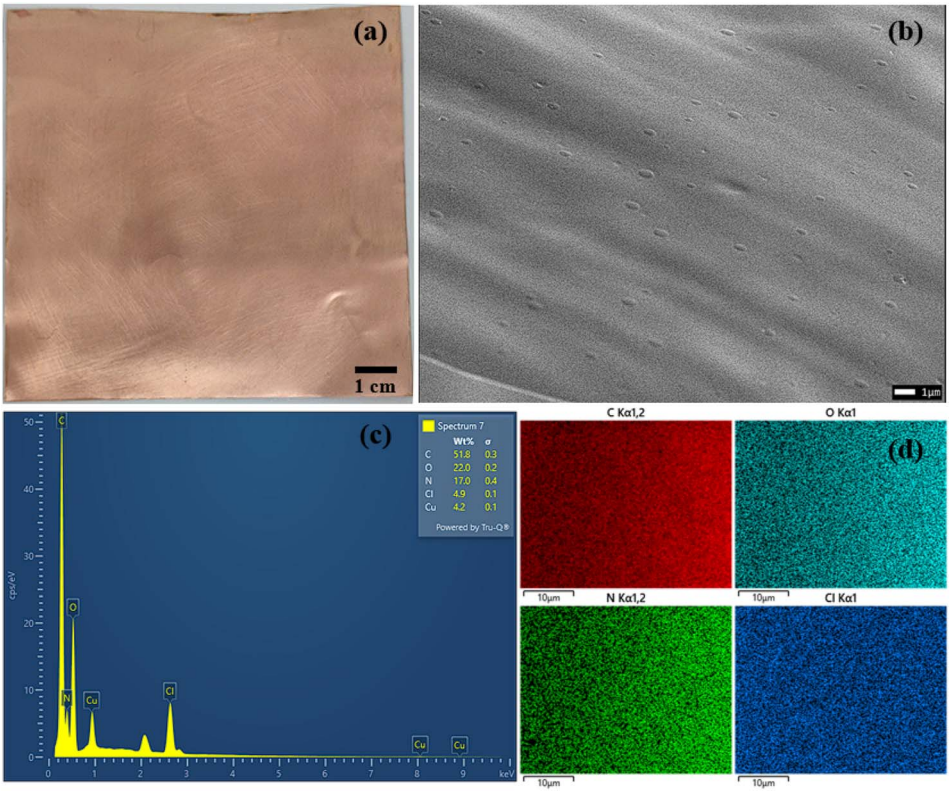

Fig. 2 (a) Appearance photo, (b) SEM, (c) EDX and (d) EDX mapping of the CS–PHMG–GA electrode prepared at CS : PHMG–GA ratio of 5 : 5.

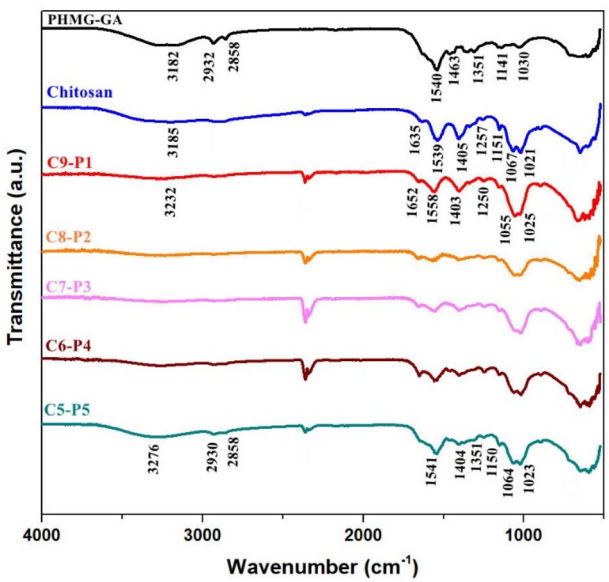

Fig. 3 FTIR spectra of pure CS, PHMG–GA, and CS–PHMG–GA composite membranes at varying CS : PHMG–GA mass ratios.

more clearly observed in Fig. 4b and Table 1, where the V_{max} value increases slightly from 313.7 V to 407.8 V, while V_{min} decreases significantly from −282.3 V to −643.2 V. As a result, the V_{p-p} value significantly increases from 596.0 V to 1051.0 V with increasing PHMG–GA content. It is well known that PHMG is a strongly cationic polymer, PHMG contains guanidine functional groups that contribute to a higher density of positive surface charges. As the amount of PHMG increases, the material surface tends to retain more positive charges. According to the triboelectric principle, when one surface becomes more positive, the opposite surface will tend to accumulate more negative charges in response. This results in V_{min} being pulled further down towards the negative side. Furthermore, the incorporation of PHMG–GA may modulate the effective Fermi level of the composite electrode surface, thereby altering the interfacial charge transfer dynamics. Specifically, a higher PHMG content enhances the material's ability to attract and retain positive surface charges during the contact phase, subsequently facilitating the transfer of a greater quantity of negative charges to the opposing FEP electrode upon separation.

Fig. 5a presents the V_{OC} output of the CS–PHMG–GA based TENG under varying humidity conditions from 40 to 90%. The voltage pulses recorded from left to right correspond to increasing humidity levels. It can be seen that the negative voltage exhibits a higher absolute magnitude compared to the positive voltage; however, both components demonstrate a decreasing trend as humidity increases. Notably, the positive voltage remains relatively stable, whereas the negative voltage undergoes a more pronounced attenuation. At low humidity levels (40% and 50%), the TENG generates strong oscillatory signals with high amplitude, achieving a peak-to-peak open-circuit voltage of up to 1470.6 V (Table 2). This demonstrates the excellent triboelectric performance of the CS–PHMG–GA

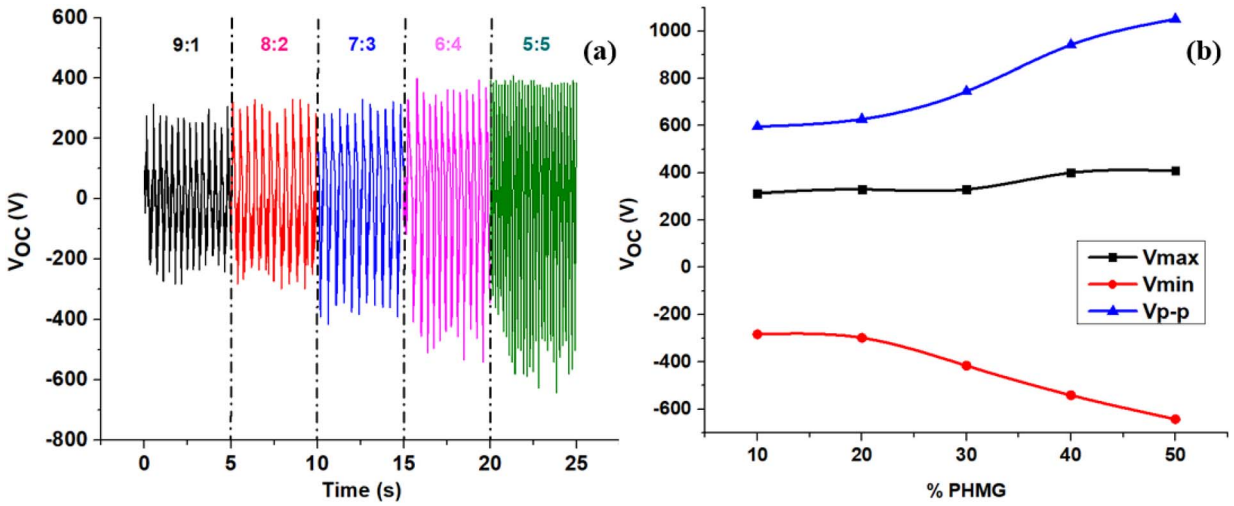

Fig. 4 (a) Open-circuit voltage V_{OC} output and (b) the V_{OC} profiles of TENG devices with CS–PHMG–GA electrodes prepared at various PHMG–GA/CS mass ratios under 70% RH.

Table 1 V_{OC} (max, min and peak to peak) of CS–PHMG–GA samples under 70% RH

Samples (CS : PHMG–GA)	V_{max} (V)	V_{min} (V)	V_{p-p} (V)
5 : 5	407.8	−643,2	1051.0
6 : 4	400.0	−541.2	941.2
7 : 3	329.4	−415.7	745.1
8 : 2	329.4	−298.0	627.4
9 : 1	313.7	−282.3	596.0

membrane. As humidity increases, the amplitude of the output voltages significantly declines, reflecting the substantial influence of humidity on the surface charge density and dielectric properties of the membrane. Nevertheless, even at a high relative humidity of 90%, the device maintains a considerable peak-to-peak V_{OC} of 862.7 V (Table 2), indicating its ability to sustain a high electrical potential output under humid conditions.

Fig. 5b and Table 2 illustrate the detailed variation of the V_{max}, V_{min}, and V_{p-p} under different humidity conditions. The declining trend of these parameters indicates a reduction in

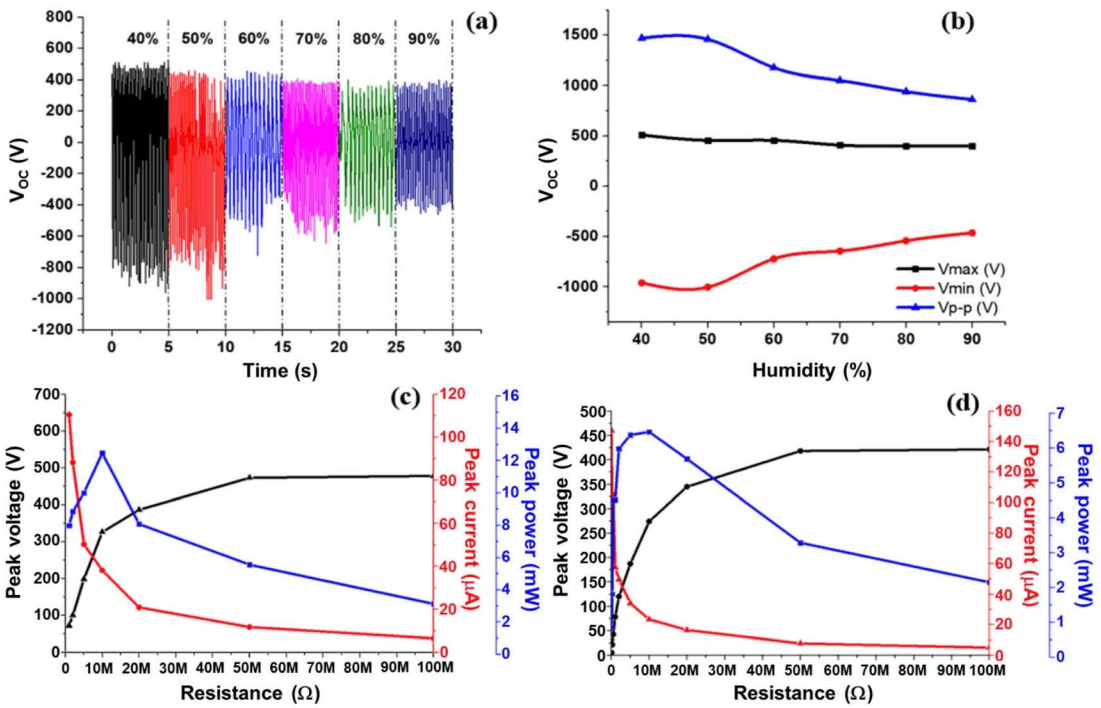

Fig. 5 (a and b) Open-circuit voltage according to operating humidity and (c and d) volt–ampere–power *vs.* resistance load characteristics at 40% and 90% humidity of C5P5-based TENG.

Table 2 V_{OC} (max, min and peak to peak) of C5P5-based TENG according to operating humidity

	C5P5 *vs.* FEP		
Humidity (%)	V_{max} (V)	V_{min} (V)	V_{p-p} (V)
40	509.8	−960.8	1470.6
50	454.9	−1003.9	1458.8
60	454.9	−721.6	1176.5
70	407.8	−643.1	1050.9
80	400.1	−541.2	941.3
90	400.0	−462.7	862.7

TENG output as humidity increases. This behavior is likely attributed to enhanced electrical conductivity of the material in humid environments, which accelerates charge dissipation. Notably, humidity predominantly influences the negative voltage component, whereas the device maintains a relatively high positive output even under high humidity (up to 90% RH).

Fig. 5c and d further investigate the power output characteristics, based on the positive pulse peak, under varying resistive loads (R) at 40% and 90% relative humidity, respectively. The voltage–current–power profiles display conventional behavior: output voltage increases with load resistance and approaches the open-circuit voltage, while output current decreases accordingly. At 40% RH (Fig. 5c), maximum power output reaches approximately 12 mW at 327 V and 38 μA with a 10 MΩ load. In contrast, at 90% RH (Fig. 5d), the peak power drops to 6.5 mW with 274.5 V and 23.5 μA at the same load. These results indicate the detrimental effect of high humidity on triboelectric performance, with reductions in output power, voltage, and current.

The underlying mechanism of this phenomenon is attributed to the increased surface conductivity under humid conditions, which hinders the accumulation and retention of triboelectric charges. Additionally, moisture may alter surface morphology and dielectric properties, thereby reducing the charge transfer efficiency during contact–separation cycles. Despite its humidity sensitivity, the CS–PHMG–GA-based TENG exhibits robust performance in high humidity environments, demonstrating its potential for practical applications.

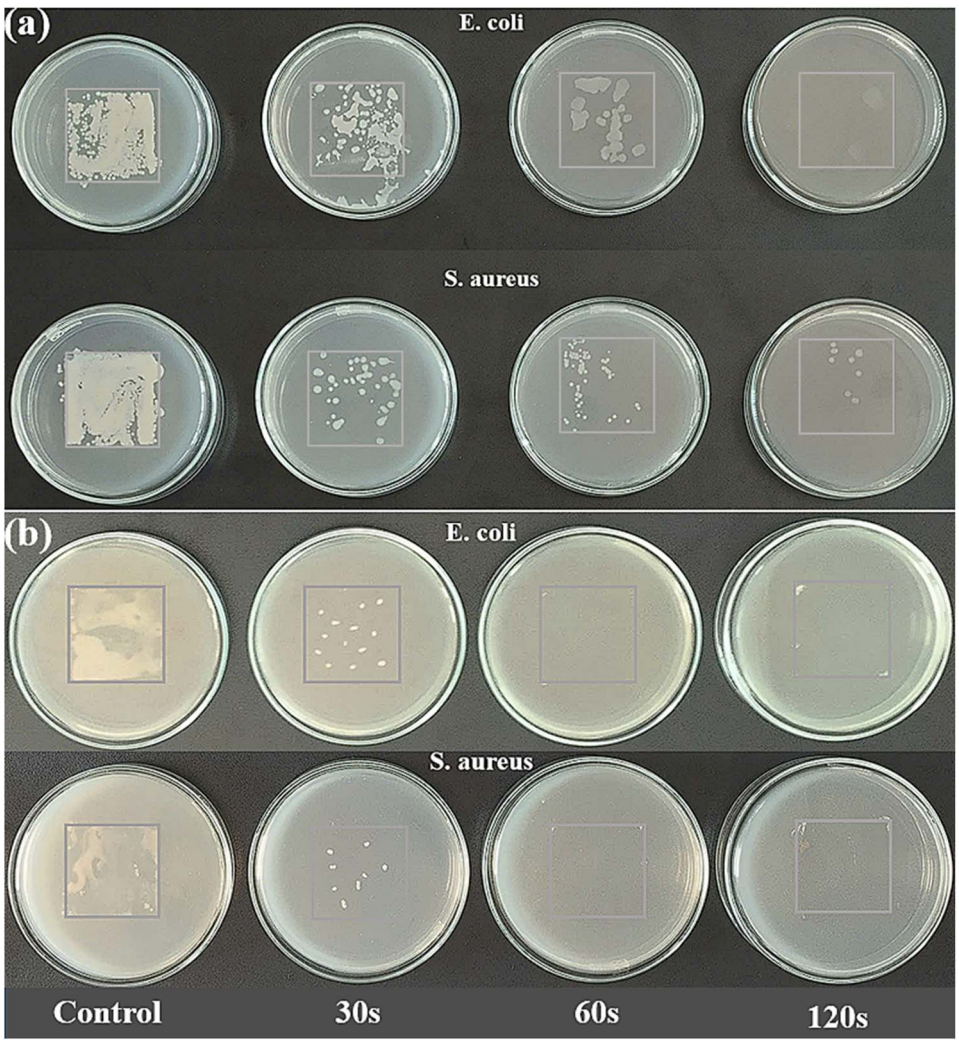

Fig. 6 Antibacterial test results of (a) Cu-based TENG and (b) C5P5-based TENG at different operation times: 0, 30, 60 and 120 seconds.

Table 3 CFU counts of *E. coli* and *S. aureus* for Cu based and C5P5-based TENGs operated over different durations

	Count (CFU mL^{-1})							
Bacteria	Cu-FEP	30 s	60 s	120 s	Cu/C5P5-FEP	30 s	60 s	120 s
E. coli	5.6×10^6	5.4×10^4	3.4×10^3	1.7×10^2	1.6×10^4	2.1×10^2	0	0
S. aureus	5.2×10^6	6.7×10^3	2.1×10^3	1.6×10^2	1.7×10^4	1.7×10^2	0	0

Antibacterial properties

The antibacterial performance of the TENG, composed of a C5P5 positive electrode (and bare Cu for comparison) and a negative electrode (FEP), was evaluated against *E. coli* and *S. aureus* under a relative environmental humidity of 90% for time intervals of 30, 60, and 120 seconds. Fig. 6 displays the results obtained after bacteria-coated positive electrodes were pressed onto agar plates for the various samples. Notably, the Cu–FEP configuration exhibited residual bacterial growth even after 120 seconds of TENG operation. In contrast, the sample with the C5P5-coated copper electrode demonstrated a marked antibacterial effect, with nearly complete eradication of bacterial colonies observed within just 60 seconds. To quantify this effect, Table 3 presents the corresponding colony-forming data. After 120 seconds of operation, the Cu-based TENG achieved an approximately 4 log reduction, decreasing *E. coli* from 5.6×10^6 to 1.7×10^2 CFU mL^{-1} and *S. aureus* from 5.2×10^6 to 1.6×10^2 CFU mL^{-1}. Despite this reduction, viable colonies were still detected, indicating incomplete bactericidal activity. In contrast, the C5P5-based TENG exhibited superior antibacterial performance. After only 30 seconds of operation, bacterial counts dropped to 2.1×10^2 CFU mL^{-1} for *E. coli* and 1.7×10^2 CFU mL^{-1} for *S. aureus.* Complete bacterial elimination (~0 CFU mL; >6 log reduction) was achieved within 120 seconds, confirming the rapid and efficient bactericidal capability of the C5P5-based TENG.

The enhanced antibacterial activity of the C5P5-based TENG can be attributed to two synergistic factors. First, the integration of the CS–PHMG–GA electrode facilitates the generation of stronger electrical pulses *via* the triboelectric effect, contributing to membrane disruption through electrostatic stimulation. Second, PHMG, a well-known broad-spectrum antimicrobial polymer,[32] can partly eliminate bacteria upon direct contact with the electrode surface. Consequently, the material exhibits a dual mode antibacterial mechanism, combining inherent biocidal activity with triboelectrically induced physical disruption.

Conclusions

A chitosan-based polymer film combined with an antibacterial polymer PHMG was successfully fabricated and employed as a positive triboelectric electrode in a TENG device. When combined with a negatively charged fluorinated ethylene propylene (FEP) film, the resulting TENG exhibited excellent electrical performance, achieving a maximum peak-to-peak output voltage of 1470.6 V and a peak power of 12 mW at 10 MΩ load under 40% RH. Remarkably, the device maintained stable operation under high-humidity conditions (up to 90% RH), still producing a high V_{OC} of 862.7 V and output power of 6.5 mW at 10 MΩ. In addition, the TENG device exhibited strong antibacterial activity, effectively eliminating *E. coli* and *S. aureus* bacteria within just 60 seconds. This combination of reliable energy harvesting in humid environments and rapid antibacterial performance suggests the potential of this TENG for practical applications in wearable electronics and hygienic interfaces, including smart face masks and self-deodorized smart shoes.

Data availability

All data supporting the findings of this study are included within the manuscript.

Author contributions

Doan T. Tung and Le T. Lu conceptualized the study, designed the methodology, and drafted the manuscript. Doan T. Tung, Hoang T. Dung, and Le T. T. Tam carried out the investigation and performed the formal data analysis. Bui V. Cuong performed the antibacterial measurements. Ha M. Dung and Duong V. Dat conducted the experiments and collected the associated data. Nguyen T. Dung prepared the CS–PHMG–GA solution. Ngo T. Dung contributed to laboratory work and provided essential logistical and administrative support. Le T. Lu and Le T. T. Tam assisted in editing and revising the manuscript. Phan N. Minh and Le T. Lu acquired funding, provided scientific guidance, and supervised the overall project. All authors reviewed and approved the final manuscript.

Conflicts of interest

There are no conflicts to declare.

Acknowledgements

This work was funded by Vietnam Academy of Science and Technology under grant number ĐL0000.08/22-24.

References

1 G. Q Gu, C. B Han, J. J. Tian, C. X. Lu, C. He, T. Jiang, Z. Li and Z. L. Wang, *ACS Appl. Mater. Interfaces*, 2017, **9**, 11882–11888.
2 J. Lin, J. Li, S. Feng, C. Gu, H. Li, H. Lu, F. Hu, D. Pan, B. B. Xu and Z. Guo, *Nano Res.*, 2023, **16**, 1052–1063.

3 X. Tian and T. Hua, *ACS Sustain. Chem. Eng.*, 2021, **9**(39), 13356–13366.
4 G. Q. Gu, C. B. Han, J. J. Tian, T. Jiang, C. He, C. X. Lu, Y. Bai, J. H. Nie, Z. Li and Z. L. Wang, *Nano Res.*, 2018, **11**, 4090–4101.
5 J. S. Meena, T. D. Khanh, S. B. Jung and J. W. Kim, *ACS Appl. Mater. Interfaces*, 2023, **15**, 29486–29498.
6 S. Cui, Y. Zheng, J. Liang and D. Wang, *Chem. Sci.*, 2016, **7**, 6477–6483.
7 F. Ejehi, R. Mohammadpour, E. Asadian, P. Sasanpour, S. Fardindoost and O. Akhavan, *Sci. Rep.*, 2020, **10**, 7312.
8 J. Liu, J. Xu, Y. Wang, Z. Li, M. Li, N. Cui, F. Zhao, L. Meng and L. Gu, *Chem. Eng. J.*, 2024, **495**, 153601.
9 J. Zhang, X. Zhao, Z. Wang, Z. Liu, S. Yao and L. Li, *Adv. Mater. Interfaces*, 2022, **9**, 2200290.
10 Y. Kim, D. Lee, J. Seong, B. Bak, U. H. Choi and J. Kim, *Nano Energy*, 2021, **84**, 105925.
11 C. Zhi, S. Shi, S. Meng, H. Wu, Y. Si, K. Zhang, S. Zhang and J. Hu, *Nano Energy*, 2023, **115**, 108734.
12 X. Lan, X. Chen, X. Chen, H. Fan, H. Zheng, H. Wang and Y. Tang, *Smart Mater. Struct.*, 2024, **33**, 045002.
13 C. M. Chiu, Y. Y. Ke, T. M. Chou, Y. J. Lin, P. K. Yang, C. C. Wu and Z. H. Lin, *Nano Energy*, 2018, **53**, 1–10.
14 X. Peng, K. Dong, C. Ye, Y. Jiang, S. Zhai, R. Cheng, D. Liu, X. Gao, J. Wang and Z. L. Wang, *Sci. Adv.*, 2020, **6**, eaba9624.
15 S. Jo, I. Kim, N. Jayababu, H. Roh, Y. Kim and D. Kim, *ACS Sustain. Chem. Eng.*, 2020, **8**(29), 10786–10794.
16 J. Tian, H. Feng, L. Yan, M. Yu, H. Ouyang, H. Li, W. Jiang, Y. Jin, G. Zhu, Z. Li and Z. L. Wang, *Nano Energy*, 2017, **36**, 241–249.
17 Q. Yan, S. Li, X. Tao, T. Wang, X. Xu, X. Wang, H. Li, X. Chen and Z. Bian, *ACS Appl. Mater. Interfaces*, 2022, **14**, 49755–49764.
18 S. Ippili, V. Jella, J. M. Lee, J. S. Jung, D. H. Lee, T. Y. Yang and S. G. Yoon, *J. Mater. Chem. A*, 2022, **10**, 22067–22079.
19 T. M. Chou, Y. Y. Ke and Z. H. Lin, *ECS Trans.*, 2017, **77**, 57–61.
20 S. Wu, G. Li, W. Liu, D. Yu, G. Li, X. Liu, Z. Song, H. Wang and H. Liu, *Nano Energy*, 2022, **93**, 106859.
21 Y. Wu, Y. Luo, J. Qu, W. A. Daoud and T. Qi, *ACS Appl. Mater. Interfaces*, 2020, **12**, 55444–55452.
22 X. Li, W. Wang, X. Lü, Y. Wang, N. Cui, B. Li, M. Ding, J. Liu, Z. Guo and L. Gu, *Nano Energy*, 2025, **134**, 110533.
23 I. Woo, D. J. Han, J. U. Yoon, S. J. Oh, W. Heo, D. H. Han, U. Nam, E. H. Sohn and J. W. Bae, *Chem. Eng. J.*, 2024, **502**, 158112.
24 D. T. Tung, L. T. T. Tam, N. T. T. Duong, H. T. Dung, N. T. Dung, N. A. Duc, P. N. Hong, N. T. Dung, P. N. Minh and L. T. Lu, *RSC Adv.*, 2025, **15**, 844–850.
25 Y. Pan, Q. Xia and H. Xiao, *Polymers*, 2019, **11**, 1283.
26 Y. Li, S. Chen, H. Yan, H. Jiang, J. Luo, C. Zhang, Y. Pang and Y. Tan, *Chem. Eng. J.*, 2023, **468**, 143572.
27 H. Shen, L. Wang, F. Zhang, J. Luo, K. Han, Z. Zhang, C. Zhang, H. Yuan, Z. L. Wang and Y. Pang, *Nano Energy*, 2025, **136**, 110677.
28 C. Yang, G. Liu, J. Chen, B. Zeng, T. Shen, D. Qiu, C. Huang, L. Li, D. Chen, J. Chen, Z. Mu, H. Deng and X. Cai, *Carbohydr. Polym.*, 2022, **282**, 119130.
29 H. M. Abdallah, M. H. A. Elella and M. M. Abdel-Aziz, *Int. J. Biol. Macromol.*, 2023, **232**, 123394.
30 Q. Zheng, L. Fang, H. Guo, K. Yang, Z. Cai, M. A. B. Meador and S. Gong, *Adv. Funct. Mater.*, 2018, **28**(13), 1706365.
31 J. N. Kim, J. Lee, T. W. Go, A. Rajabi-Abhari, M. Mahato, J. Y. Park, H. Lee and I. K. Oh, *Nano Energy*, 2020, **75**, 104904.
32 D. T. Nguyen, L. T. Pham, Ha T. T. Le, M. X. Vu, H. T. M. Le, H. T. M. Le, N. H. Pham and Le T. Lu, *RSC Adv.*, 2018, **8**, 19707–19712.